CHAPTER-4

STRUCTURAL DETERMINATION OF CHARGE EXTRACTION INTERFACES USING XRR TECHNIQUE

4.1 Introduction

In OPV devices, the interfacial layers, and their interfaces with active layers and respective electrodes are beneficial to tune the energy level alignment, to tailor the built-in electric field, to improve charge selectivity, to alter the morphology of active layer by modifying surface energy and to achieve good interfacial stability. Thus, the performance of OPV devices largely depends on materials of interface layers, and their structural, electronic and optical properties. An understanding of the correlation between structure and these properties on interfacial layers is highly desired. However, in bulk-heterojunction OPV devices such study becomes exciting as well as challenging due to a complex nature of interfaces. The BHJ active layer and interface layer junction have a 3-dimensional interface with a complex distribution of molecular spacing and relative molecular orientation at the interface. The electrical characterization parameters with a localized morphological characterization techniques (*e.g.* AFM, SEM, and TEM) are, in general, used to investigate interfaces in OPV devices[193]. However, these characterization techniques enable us to investigate lateral morphology on nano-scales. Recently, neutron reflectivity (NR), X-ray reflectivity (XRR) and X-ray photoelectron spectroscopy (XPS) techniques have been used to study vertically buried interfaces and their structure within OPV devices.[194-198] The NR and XRR techniques are very promising to study the grain size distribution, roughness at the interfaces and the density profile of thin films along the path light travels in OPV devices.[199-201]

The properties of hole/electron interlayers and their interfacial interaction with bulk heterojunction active layer are of significant importance to realize high performing OPV devices. Recently, Ou *et al* has reported PC61BM rich surface near ZnO interface through electrochemical studies and suggested the filling of pinhole pathways in sol-gel processed ZnO.[202] However, in general, the sol-gel processed ZnO thin films have shown a compact granular structure having lesser leakage pathways.[49,97] So further non-destructive structural characterization was needed to investigate the evolution at interfaces. In this report, structural characterizations have been demonstrated to understand physical mechanisms at the interface of BHJ of PTB7-Th:PC71BM and sol-gel processed ZnO. The interfaces in PTB7-Th:PC71BM based inverted OPV devices are investigated using X-ray reflectivity (XRR) technique.

The optical density (δ) for a thin film can be defined as;

$$\delta = \frac{2\pi\rho r_0}{k^2} \qquad \text{.....(1)}$$

Where, ρ is the electron density, r_0 radius of the electron (Thomson scattering length), and k is the momentum vector ($k = 2\pi/\lambda$).

The experimental data obtained from XRR measurement was then fitted with Parrot's recursive formula under the assumption of negligible absorption loss of X-ray due to the different layers and the refractive index of the thin film is given as;

$$n = 1 - \delta + i\beta \quad \text{.....(2)}$$

Where, n is the refractive index, a material property, δ is the optical density, and β is the absorption loss.

The present chapter focuses on the structural investigation of ZnO/BHJ and BHJ/MoO_x interfaces in inverted OPV devices by utilizing optical contrast in various layers. We explored the interface layer formation between BHJ and electron/hole charge transport layers using XRR. AFM is also performed on ZnO and BHJ thin films to support the findings of XRR. We first describe the sample preparation and then the XRR measurement and its analysis in order to get the structural information across the sample depth.

4.2 Experimental section

In order to probe structural features present at each interface in OPV device shown in figure 4.1, three specific thin film samples were fabricated on ITO coated glass substrates in ambient condition with the structure of ITO/ZnO, ITO/ZnO/BHJ, ITO/ZnO/BHJ/MoO_x having the similar thin film thicknesses as they were on the actual device. Pre-cleaned indium tin oxide (ITO) coated glass substrates as explained in the chapter-2 were kept in a UV-Ozone treatment system for 25 minutes in order to increase their hydrophilicity and to remove any residual contamination. An electron selective contact (Cathode interface layer) on ITO, ZnO thin film, was prepared as previously reported[97]. The ZnO thin film thickness was about 40 nm confirmed by Dektek surface profiler. For ITO/ZnO/BHJ sample, on top of ZnO thin film, a thin layer (~ 25 nm) of PTB7-Th:PC71BM BHJ was deposited from its solution in ODCB/DIO (97:3, v/v) spun at 5000 rpm for 60 sec[49]. The thickness of the active layer was kept lesser so that the absorption effect layer can be restricted to have appropriate XRR fringes. Further, a thin film of MoO_x (~ 10 nm) was coated on ITO/ZnO/BHJ sample to fabricate the third sample ie, ITO/ZnO/BHJ/MoOx.

XRR and AFM measurements were performed on each sample. The XRR measurements were carried out at the reflectivity beamline BL-4 at INDUS 1, Indore, India

with the wavelength of 80 Å. Reflectivity beamline is comprised of a grazing incidence Toroidal Grating Monochromator (TGM) and toroidal mirrors for pre- and post- focusing optics. The beamline is designed to cover 40 – 1000 Å photon wavelength range. Further details of the beamline are given in the report by Nandedkar *et al.*[165]. The experimental station in this beamline is a high vacuum reflectometer, comprised of the t-2t goniometer and a z-translation stage to keep the sample in and out of direct beam[166]. A silicon XUV photodiode is used to measure reflected beam intensity.

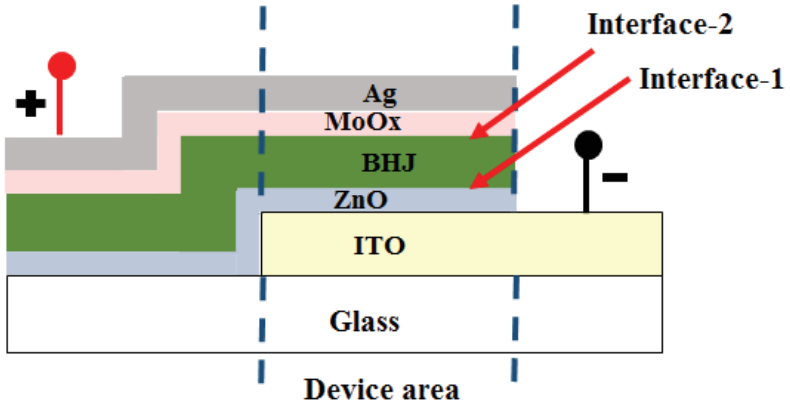

Figure 4.1. Inverted OPV device architecture and its interfaces under probe.

4.3 Results and Discussions

4.3.1 X-ray reflectivity measurements

In order to understand structural properties at various interfaces in our device, we performed XRR measurements on ITO (S1), ZnO/ITO (S2), BHJ (PTB7-Th:PC71BM)/ZnO/ITO (S3), and MoO_x/BHJ/ZnO/ITO (S4) layered structures using soft X-rays of wavelength 80 Å. The normalized reflectivity profiles for these four samples are shown in figure 4.2 and corresponding optical density (δ) in figure 4.3. Every sample shows distinct profile pattern as the thickness of each layer is dissimilar along with the contrast in optical density between layers. Optical density has been derived for each layer by fitting the XRR data using Parratt's recursive method[163-164,203]. The parameters obtained on the best fits of the data for different samples have been summarized in table 1. These samples were prepared on the glass as a base substrate and the thickness of layers was kept same as in working device except BHJ layer. The BHJ layer thickness was reduced to the limits of XRR measurements keeping other parameters same as an active device. The ITO on glass was used as the bottom electrode

in the device structure for which XRR fitting has been done for the layer with a thickness of ~ 130 nm, while bottom glass considered as an infinitely thick base layer. The optical density of the ITO layer was found to be 0.022 with a thickness of 129.45 nm. Similarly, the best fit for sample S2 was observed as per theoretical values of ZnO layer for which the optical density was obtained as 0.014 with a layer thickness of 38.09 nm. In the case of S3, the best fit was obtained only upon an introduction of an extra layer between ZnO and BHJ layers, mentioned as interface layer-1 (IL-1) in table 1. The thickness of this layer (IL-1) was found to be about 4 nm with an interfacial roughness of 0.6 nm. Thus we observed a signature of additional intermixing layers at the interfaces of ZnO/BHJ for which optical density is close to the ZnO layer. In the case of S4, again another interface layer, termed as IL-2, was inserted in order to get the best fitting. The existence of IL-2 was in between MoO_x and BHJ layer and the thickness was ~ 8.2 nm with an interfacial roughness of about 5.6 nm. The optical density of this layer (IL-2) was found to be 0.014. The origin of the IL-1 layer may be resulted due to the planarization of ZnO layer surface roughness by downward percolation of PC71BM small molecules, as reported by Ou *et al.*[202] and Hussein *et al.*[204]. While IL-2 may be originated due to molecular interdiffusion between adjacent organic-inorganic layers. The thermally evaporated MoO_x molecules generally have the island-like feature on the organic BHJ surface reported elsewhere[205]. Due to which, the high roughness was observed for the IL-2 layer. Also, the IL-2 layer is MoO_x rich as the optical density of this layer is close to MoO_x layer. The fitted XRR parameters show smoothening of interfacial junctions which contribute to the improvement of parasitic resistances of the OPV device. It also supports the lowering of the recombination of a free charge carrier thereby better collection of these charges at the respective electrodes. Such change at the interlayers of the devices contributes to improvement in device efficiency.

Table 4.1. OPV device sub-layer/layer thickness with corresponding interfacial roughness (σ) and optical density (δ) extracted from XRR fitting.

Samples	Layer from top surface	Layer thickness (nm)	Optical density ($\delta \times 10^{-3}$)	Layer surface roughness (nm)
S1	ITO	129.45±0.31	22.00±0.05	4.74±0.01
S2	ZnO ITO	38.09±0.30 129.45±1.04	14.00±0.11 22.00±0.18	3.36±0.03 4.74±0.04
S3	BHJ IL-1 ZnO ITO	22.17±0.09 4.07±0.02 35.00±0.14 129.45±0.52	8.00±0.03 12.00±0.05 14.00±0.06 22.00±0.09	4.47±0.02 0.60±0.00 1.99±0.01 4.04±0.02
S4	MoOx IL-2 BHJ IL-1 ZnO ITO	5.48±0.24 8.20±0.36 17.9±0.79 4.07±0.18 35.00±1.54 129.45±5.70	16.00±0.70 14.00±0.62 8.00±0.35 12.00±0.53 14.00±0.62 22.00±0.97	4.07±0.18 5.59±0.24 4.75±0.21 0.45±0.02 0.99±0.04 4.04±0.18

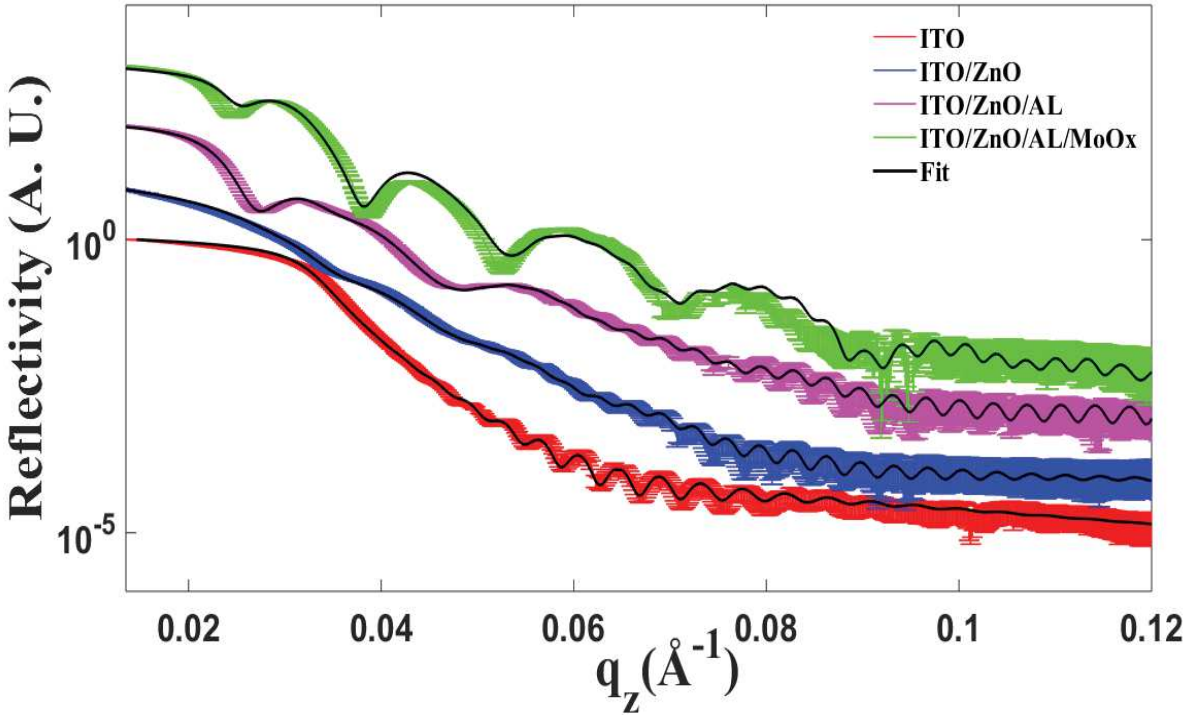

Figure 4.2. X-ray reflectivity data for the samples S1, S2, S3 and S4 with fitted profile shown in solid line.

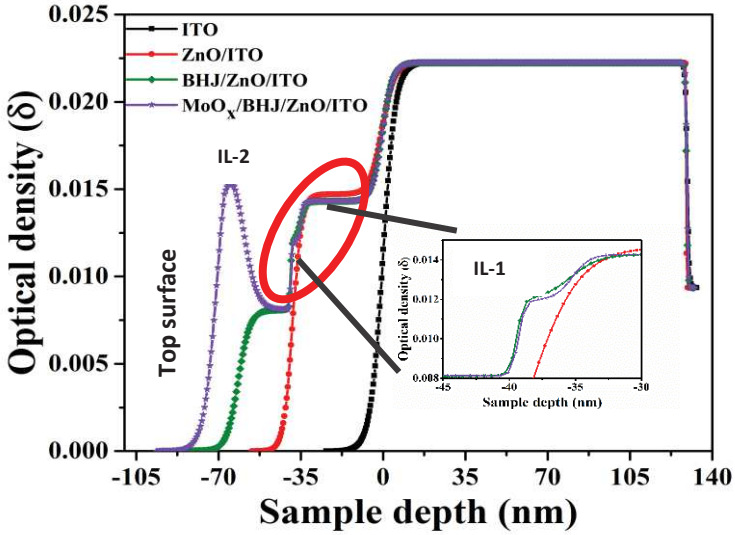

Figure 4.3. The optical density profiles for the samples S1, S2, S3, and S4. IL-1 is shown in the zoomed picture (inset).

4.3.2 Topography measurements

To support the findings of XRR measurement, further AFM measurement has been performed for ZnO and BHJ thin films. The surface topography, shown in figure 4.4 (a) for ZnO layer and in figure 4.4 (b) for BHJ layer, shows average roughness of ZnO surface as 1.8 nm and 2.2 nm for BHJ surface. These roughness parameters, obtained from AFM measurement, had nonconformity from the results of XRR measurement. This may be because AFM technique provides microscopic measurement while XRR technique allows macroscopic capacity. But the surface roughness at ZnO indicates that there is possibility of intermixing of ZnO and PC71BM molecules as PC71BM has tendency to percolate downwards. On the other hand, the presence of polymers, as expected, at the surface may lead to molecular interdiffusion of thermally evaporated MoOx molecules. Figure 4.4 (c) shows the suface totpography of MoOx thin film on top of BHJ active layer after the planarization. The roughness MoOx thin film has been observed about 4.2 nm quite close to the value obtained from XRR results.

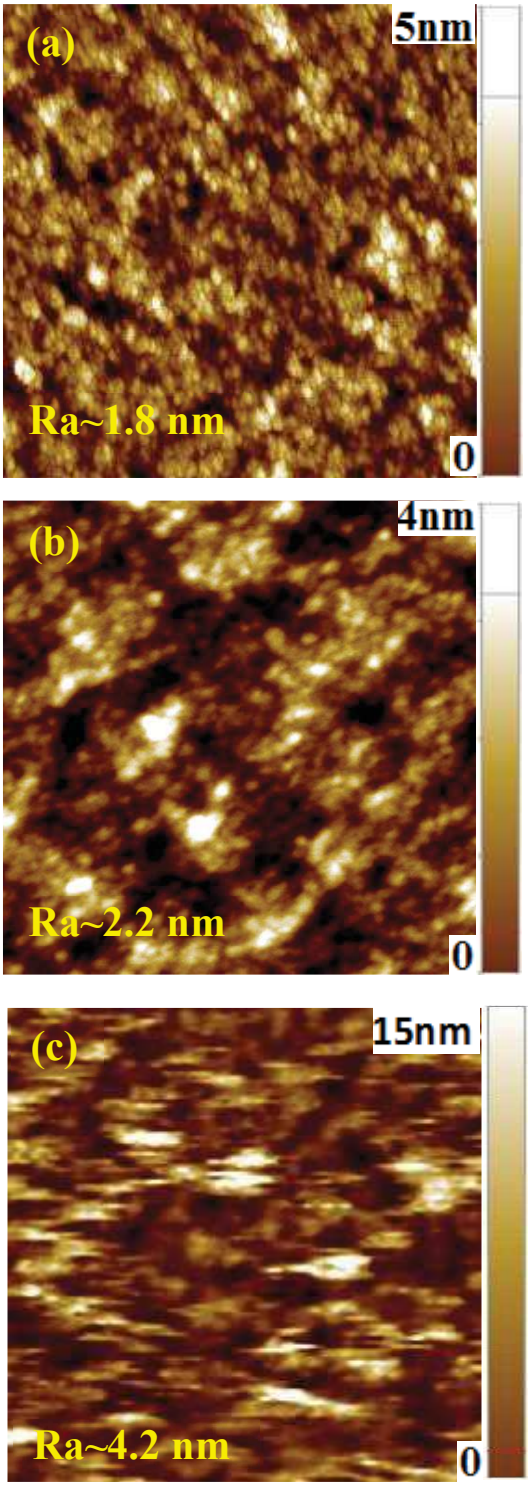

Figure 4.4. (a) Surface topography of ZnO thin film on ITO/Glass substrate, (b) Surface topography of BHJ thin film on ZnO/ITO/Glass substrate, and (c) Surface topography of MoO_x thin film on BHJ/ZnO/ITO/Glass substrate

4.4 Conclusions

We used a non-destructive technique XRR to investigate the buried planar interfaces at the ETL(ZnO)/BHJ and the HTL(MoO_x)/BHJ heterojunctions in PTB7-Th:PC71BM based OPV devices. The XRR analysis at the ZnO/BHJ and MoO_x/BHJ interfaces provides the much better structural information and hence the implications for OPV device interface engineering. The smoother interfaces at ETL/BHJ and HTL/BHJ heterojunctions facilitate better charge transport leading to less charge accumulation which eventually prevents the recombination losses in our devices. The large value of recombination resistance (~ 5 kΩ-cm^2 at 0V) and electron lifetime (~ 70 μs at 0V) for the OPV devices extracted from impedance measurement discussed in the previous chapter suggest good phase mixing in BHJ active layer and smooth ETL/BHJ and HTL/BHJ interfaces. We believe our results have great importance to understand the structure of buried planar interfaces at ETL(HTL)/BHJ and their connection with the electrical parameters representing various interfacial mechanisms in OPV devices.

In summary, on the basis of the above discussions, the microscopic features of bulk heterojunction OPV device is schematically shown in figure 4.5. The inter-diffusion of MoO_x in PTB7-Th dominant portion of bulk heterojunction and infusion of PC71BM on ZnO layer smoothen HTL and ETL interfaces, respectively. Such modification at interfaces provides us a better picture of the physical phenomenon in the device.

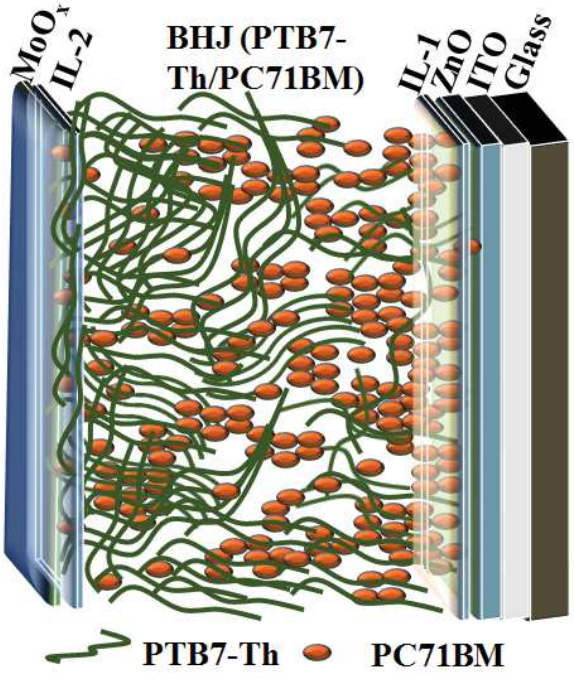

Figure 4.5. The schematic of OPV BHJ device layers and interfaces IL-1, IL-2.

The ideal structure of BHJ in organic solar cells consists of interspaced phases of donor polymers and acceptor molecules within the limits of 10-20 nm exciton diffusion length, the donor, and acceptor phases should be interdigitated across the active BHJ for efficient charge transport and less recombination, and finally the presence of pure donor phase at HTL and pure acceptor phase at ETL to reduce the recombination losses.[206-208] The schematic predicted from XRR analysis, in figure 5, shows the extent of the possibility of getting ideal BHJ solar cells through self-assembly of donor polymers. Numerous work had been reported for getting ideal structure of BHJ layer in OPV devices by using various solvent processed, inorganic templates, and nanostructures.[209-212] In coming chapters, we will be discussing the novel approach towards modifying the interface between ETL and BHJ layer with the help of understandings from XRR analysis.